Journal of Engineering Science and Technology Review 16 (2) (2023) 100 - 106

Research Article

JOURNAL OF
Engineering Science and Technology Review

www.jestr.org

Non-subsampled Shearlet Domain-based De-speckling Framework for Optical Coherence Tomography Images

Pradeep Kr. Gupta[1,*], Amit kr. Chanchal[2], Shyam Lal[3] and Vivek Gupta[4]

[1]*Pranveer Singh Institute of Technology, Kanpur-209305, Uttar Pradesh, India*
[2]*Kolhapur Institute of Technology's College of Engineering(Autonomous),Kolhapur,Maharashtra, India*
[3]*National Institute of Technology Karnataka, Surathkal, Mangaluru-575025, Karnataka, India*
[4]*G L Bajaj Institute of Technology &Management Greater Noida, U.P., India*

Received 28 September 2022; Accepted 28 March 2023

Abstract

An effective instrument for obtaining an image of the retina is an optical coherence tomography (OCT) imaging device. OCT images of the retina are useful for diagnosing and tracking eye diseases. However, different physical configurations in the imaging apparatus are to blame for the speckle noise in retinal OCT images. The OCT image quality and assessment reliability are reduced due to aforementioned noise. This paper offered a paradigm for reducing speckle noise that was motivated by the mathematical formulation of speckle noise. Two distinct noise components make up speckle noise, one of which is additive and the other of which is multiplicative in nature. For each sort of noise, the suggested structure employs a different filter. To reduce the additive component of speckle noise, Weiner filtering is used. To minimize the multiplicative component of noise, a particular arrangement based on non-subsampled shearlet transform (NSST) is used. It is now widely acknowledge that NSST overcome the limitations of traditional wavelet transform therefore it very useful in dealing of distributed discontinuities therefore it is prefer in this research work .Real retinal OCT pictures are used to assess the proposed framework's quantitative and qualitative performance. The PSNR, MSE, SSIM, and CNR metrics are used to compare the suggested framework. In comparison to existing cutting-edge filters, the proposed framework performs better in terms of noise suppression capability with structure preservation capabilities. The proposed technique gives highest PSNR, SSIM and CNR value that indicate the effectiveness of proposed work in addition to this proposed work give lowest MSE value. The proposed work give better enhance images in comparison to other existing filter therefore it may be helpful to find out any abnormality in OCT image and improve the diagnose of OCT retinal image.

Keywords: OCT, Non-Subsampled shearlet transform (NSST), Wiener filter,enhancement, CNR

1. Introduction

OCT is an extremely useful tool for obtaining microscopic-resolution pictures of the retina. OCT imaging is a potent imaging technique for the identification of numerous illnesses, including glaucoma [1, 2] and age-related macular degeneration (AMD) [3-6]. This is due to the non-invasive nature of OCT imaging. A helpful biomarker for identifying and diagnosing disorders associated with the retina is the measurement of OCT image layer thickness. However, the speckle noise in OCT images degrades the image quality and makes it challenging to conduct an accurate evaluation of OCT images. As a result, the most crucial stage in the examination of OCT pictures is image enhancement. In OCT images, speckle noise appears as a grainy pattern. The imaging system's wavelength is the only factor that influences this kind of noise. The textural properties and clinical features necessary for image analysis are also contained in the speckle noise. As a result, a crucial stage in the OCT enhanced imaging system is the separation of the noise component from the information component.

1.1. OCT Images

Like Ultrasound imaging, Optical Coherence Tomography (OCT) is also animportant imaging technique used for ophthalmology and retinal imaging. Currently, OCT has been a powerful tool for the diagnosis of retinal-related disease. It provides a high-resolution cross-sectional view of the retina. Measurement of retinal layer thickness from OCT image helps in the clinical diagnosis of various retinal diseases. For identification and assessment of retina abnormalities ,Optical Coherence Tomography (OCT) is the most valuable diagnostic imaging. OCT is a non-invasive imaging technique relying on low coherence interferometry to generate in vivo, cross-sectional imagery of ocular tissues. Cross-sectional visualization is an extremely powerful tool to find out abnormality in retinal images. Optical Coherence Tomography generates cross sectional images by analyzing the time delay and magnitude change of low coherence light as it is backscattered by ocular tissues. An infrared scanning beam is split into a sample arm (directed toward the subject) and a reference arm (directed toward a mirror). As the sample beam returns to the instrument it is correlated with the reference arm in order to determine distance and signal change via photodetector measurement.

*E-mail address: er.pradeepgupta@gmail.com
ISSN: 1791-2377
doi:10.25103/jestr.162.13

2. Literature Review

Numerous de-speckling filters have been developed in the literature to reduce the speckle noise in OCT pictures. OCT images can also benefit from some de-speckling filters that are utilized for SAR images [7-9]. Adaptive filtering performs better than other filtering methods for OCT pictures. This filtering method alters pixel intensity by gathering data from the area surrounding the pixel under consideration. The concept of adaptive filtering technique is employed with the hybrid median filter [10], homomorphic Wiener filter [11], enhanced Lee filter [12], symmetric nearest neighbour filter [13], and kuwahara filter [14]. In OCT pictures, wavelet-based filters perform better after the concept of adaptive filtering. According to a literature review, wavelet denoising with multiscale resolutions is more effective for enhancing OCT images. Shift-invariant wavelets are used by Ozcan et al. [15] to reduce speckle noise. Speckle noise in OCT pictures is also removed using a spatially adaptive wavelet filter. The system mentioned above computes a variety of coefficients to determine threshold values [16]. A wavelet method was also used by Mayer et al. [17] to reduce the impact of speckle-noise in OCT pictures. In the method described above, coefficients are calculated by gathering data on the noise pictures' structure.

Some Researchers used the diffusion technique to improve OCT images once the adaptive filter was created. With the preservation of the fine structure of the photographs, these techniques can smooth the images. Ordinarily, diffusion procedures are developed for partial differential equations (PDEs). Salinas et al. [18] offered a comparison of the Perona-Malik isotropic diffusion filter and the nonlinear complex diffusion filter for OCT image denoising. Jinming Duan et al. [19] also suggest a second-order total generalized variation (TGV) decomposition approach to minimize speckle noise in OCT pictures. The OCT pictures are denoised using the aforementioned approach, which uses TGV regularization. The staircase side effects do not appear in the output photographs.

Two adaptive spatio-temporal approaches have been put forth by Katsaggelos et al. [20] to reduce the noise in the image. Images are filtered using three cascading 1-D estimators. With regard to discontinuities, the estimator response is adaptive. A signal is divided into a stationary and a non-stationary portion based on the most recent statistics. visual outcomes Show that this filter produces better results for images with high SNR values; nevertheless, the recursive version produces comparably better results for images with low SNR values. By gathering data on the local coherence of the retinal structure, Fernández et alalgorithm .'s [21] automatically determined the thickness of the retinal layer. The method mentioned can help photos become noise-free. With this method, we can quickly determine the RNFL layer thickness for illness identification. An image enhancement algorithm was created by Anantrasirichai et al. (2014) [22] for the detection of RNFL thickness in the OCT input pictures. The suggested method smooths the output image by applying wavelet thresholding, bilateral adaptive-weighted filtering, and intensity modification. The adaptive weights are calculated using local entropy. We achieve improved glaucoma detection precision and picture quality.

The bilateral filter with adaptive iteration has been used by Sudeep et al. (2016)[23] to minimise the speckle noise in OCT images. The OCT image's visual quality is enhanced by the employment of a bilateral filter. After averaging the filtered data, a denoised OCT image is produced. Experimental findings indicate that the suggested technique performs better. A two-dimensional filter for noise reduction in OCT pictures has been presented by Mirzapour (2016) [24]. The method described above can be used to extract spectral and spatial-temporal properties from images. A wave atom transform-based Shrinkage Filter was proposed by Yongzhao Du et al. [25]. In this method, the OCT pictures were despeckled using cycle spinning technique. All of the image's features are preserved by the suggested filter. The technique is more complicated, but the noise strength is controlled by a single variable parameter.

The K-SVD dictionary learning strategy is used by Raheleh Kafieh et al. [26] to enhance the effectiveness of the de-speckling technique. The Dual Tree Complex Wavelet Transform performs better when using this learning strategy. The aforementioned method offers flexibility in vocabulary learning for noise reduction but requires a lot of time. Total Generalized Variation (TGV) for OCT images is described by Jinming Duan et al. in their study [27]. The OCT pictures are despeckled using the Bregman algorithm approach. The staircase side effect is eliminated from the final image by this procedure.

By using variational image decomposition, Hongwei Ren et al. [28] are able to distinguish the cartoon texture from the noise portion of the original OCT image. Curvelet space describes the noise in the image, while Hilbert space represents the texture. The suggested approach can conduct edge detection, image segmentation, and layer thickness computation. The OCT pictures are de-speckled using a variety of ICA algorithms, including RUNICA, JADE, Fast ICA, and SOBI, according to Ahmadreza Baghaie et al. [29]. SOBI performs better due to different techniques. A nonlinear transform-based strategy using the Gaussian distribution as the probability distribution function was proposed by Zahra Amini and Hossein Rabbani [30]. The calculation of an image's histogram in this method uses a Normal-Laplace mixing distribution. The Gaussian assumption produces more accurate findings, according to experiments. The intraretinal layer's precision is enhanced by this method. To locate a similar area in OCT images, Leyuan Fang et al. [31] use the Sparse reconstruction method for layer segmentation. The rectangular patch is used in the suggested method to provide a better approximation of the image.

The following describes the other sections of the paper: In Section 3, the suggested framework is explained. The material and methodology utilized in the proposed framework are explained in Section 4; the results of the proposed framework are compared with those of other compared filters in Section 5. The conclusion and future application of the suggested framework are provided in section 6.

3. Proposed Framework

The analysis of the literature confirms that there are two types of speckle noise in the OCT image. One of two elements has an impact on the image that is additive, whereas the other has an impact that is multiplicative. The suggested methodology treats each of these elements separately. In this approach additive part of speckle noise is remove by Weiner filtering, and non-subsampled shearlet transform (NSST) is used to reduce the multiplicative factor of speckle noise.In this algorithm, first, Wiener filtering is applied on the noisy image; after that NSST transform decomposes the filtered image in low frequency and high-frequency components. A diffusion process is used for low-frequency components and thresholding is applied to high-frequency components. In the last by the inverse operation, we get the denoised image.The suggested framework's process flow is depicted in Fig. 1.

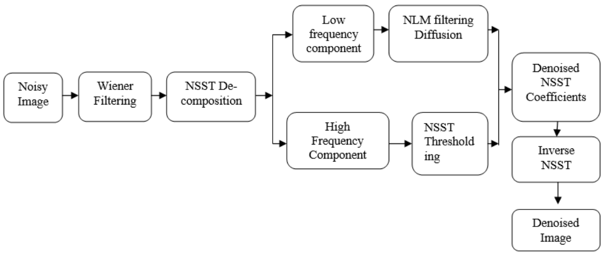

Fig. 1. Process Flow of proposed Framework.

3.1. Speckle Noise Modelling

Many studies suggest that the noise shown in retinal OCT pictures has two components. Although the second component of noise has a multiplicative influence on the original image, the first part of noise is additive in nature. Equation can be used to depict a noisy OCT image (1) [32]

$$I_d(x,y) = I_o(x,y).N_m(x,y) + N_a(x,y) \quad (1)$$

here, $I_d(x,y)$ is represents degraded image by speckle noise, $I_o(x,y)$ is the noise-free image. $N_m(x,y)$ is the multiplicative part of the noise and $N_a(x,y)$ is the additive part of the noise. The proposed framework is based on the concept of different noise requiring different filters to reduce this type of noise.

3.2. Wiener Filtering

Consider a image corrupted by speckle noise define in eq.(2):

$$I_d(x,y) = I_o(x,y).N_m(x,y) + N_a(x,y) \quad (2)$$

Now the goal of the Wiener filter is to reduce the additive part$N_a(x,y)$ of speckle noise. Wiener filter reduces the additive component of the noise by estimating the mean square error between estimation value and original value defined as in eq. (3):

$$MSE(I_o) = \frac{1}{N}\sum_{x,y=1}^{N}(\hat{I_o}(x,y) - I_o(x,y))^2 \quad (3)$$

where N is the number of elements in the input image. In this proposed work $N_a(x,y)$ and $I_o(x,y)$ are the Gaussian process, therefore estimation by wiener filter have a straightforward scalar form as in eq. (4)

$$\hat{I_o}(x,y) = \frac{\sigma_I^2(x,y)}{\sigma_I^2(x,y)+\sigma_n^2(x,y)}[I_d(x,y) - \mu_I(x,y)] + \mu_I(x,y) \quad (4)$$

Where σ^2 and μ are the variance and means of the image, respectively. To use the above equation, we need to determine $\sigma_I^2(x,y)$ the estimation of noise-free image.

3.3. Non-Sub Sampled Shearlet Transform (NSST)

The non-sub sampling shearlet transform is used in the proposed work to minimize the multiplicative noise component of speckle noise. Wavelet - based transform is a milestone in multiscale transform, and non-sub sampled shearlet transform is a subcategory of multiscale transform [33]. Wavelet transform can be used to quickly resolve the high-dimensional signal singularity problem [34]. It is not, however, appropriate for images. Curvelet and contourlet transforms have recently been used to resolve these issues [35]. The decomposition of an image in several directions is the fundamental tenet of these transforms. The Gibbs phenomenon [36] is a result of the breakdown process in the enlarged image. This flaw is eliminated via the shearlet transform (ST). The multidimensional and multidirectional extension of an average signal is provided by the shearlet transform. The shearlet wave is mathematically described as follows in the 2D-affine system:

$$AS_{2D} = \{\psi_{k,l,m}(x) = \left|det\, A^{k/2}\right|\psi(slA^k x - m): k,l \in ,Z, m \in Z^2\} \quad (5)$$

where A-is a multiscale decomposition matrix, S-is a multidirectional shear matrix, k- is the decomposition scale, l- is the direction parameter, m- is the translation parameter.

In $L^2(R^2)$ the domain, the basis function $\psi_{k,l,m}(x)$ is calculated by a single-window function with good local characteristics. Shear matrix S is a responsive for the selection of shearlets.

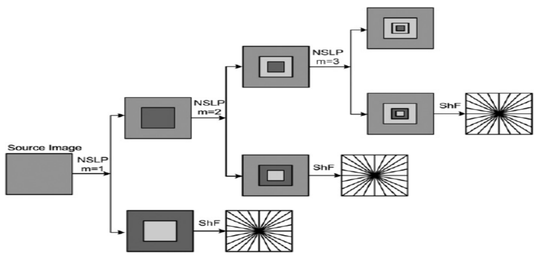

Fig. 2. Decomposition of the source image for D=3 by NSST.

The image decomposition is carried out by Cunha and Do[37] using the non-subsampled laplacian pyramid (NSLP) filter. For the multiscale and multidirectional decomposition, NSST uses NSLP and Shf. An input image is divided into a high-frequency and a low-frequency subimage during the NSLP decomposition process. The low-frequency subimage is then iteratively dissected after that. An picture is divided into D+1 subbands at any random decomposition level D. These decomposed photos and the source images are both the same size. One of these sub-images has a low frequency, while the other D sub-images have high frequencies. In order to decompose the high-frequency sub-images without subsampling, ShF is also using NSST decomposition. At each level of decomposition, NSLP generates the high-frequency subband images for a given level L, and 2K directional subband image coefficients are produced. The NSLP and its accompanying directional decompositions are depicted in Fig. 1 together with a three-level NSST decomposition. In this work, three layers of image decomposition are used to shear an image in the following numbers: 8, 8, and 4 from finer to coarser scale.

3.4. NSST Thresholding

Different authors proposed various thresholding method for image denoising. Out of these various thresholding methods, the proposed method applies hard thresholding with NSST.

The following step explains the flow process of the proposed algorithm:

Step 1. Wiener filtering is used to reduce the additive noise part from the denoised image.
Step 2. Apply the NSST decomposition on Output of step 1.
Step 3. NLM filtering and diffusion process are applied on low-frequency sub-image.
Step 4. NSST thresholding is applied to high-frequency components.
Step 5. NSST Denoised component are obtained.
Step 6. Inverse NSST applies to obtain the denoised image.

3.5. Image Database

For the conduction of the experiment, the OCT images are chosen from the Mendeley database (https://data.mendeley.com/datasets/rscbjbr9sj/2)

3.6. Quality Metrics

In this proposed de-speckling framework PSNR, MSE, SSIM and CNR quality metrics are used for performance analysis. PSNR is a measure of the image enhancement capability of any de-speckling technique. PSNR is defined as

$$PSNR(dB) = 10\,log_{10}\left(\frac{I_{max}^2}{MSE}\right) \tag{6}$$

Where I_{max} is the input signal maximum power. High PSNR value is desirable for a better method.

Mean square error (MSE) is an indication of noise in the output image after the denoising process. MSE is defined as:

$$MSE = \frac{1}{AB}\sum_{r_1=0}^{A-1}\sum_{r_2=0}^{B-1}\left(P_d(r_1,r_2) - P_n(r_1,r_2)\right)^2 \tag{7}$$

$P_d(r_1,r_2)$ and $P_n(r_1,r_2)$ are the output and input values for an image of order $A \times B$. The lower value of MSE is desirable for a better de-speckling method.

Structural Similarity Index (SSIM) measured the structural similarity between the noisy image and the denoised image. SSIM is defined as [27].

$$SSIM(I,O) = \frac{(2\mu_I\mu_O+c_1)(2\sigma_{I,O}+c_2)}{(\mu_I^2+\mu_O^2+c_1)(\sigma_I^2+\sigma_O^2+c_2)} \tag{8}$$

I and O indicate the input and output image, $\mu_I, \sigma_I^2, \mu_O, \sigma_O^2$ and $\sigma_{I,O}$ are mean, variance, covariance values for noisy and denoised images, respectively. (c_1,c_2) are constants for equation stabilization factors.

For the de-speckling framework, contrast to noise ratio (CNR)[39] is another good indication of quality. This setting computes the contrast between the ROI that was chosen and the image's noisy backdrop. It's described as:

$$CNR = \frac{1}{N}\left[\sum_{n=1}^{N}\frac{\mu_n-\mu_b}{\sqrt{(\sigma_n^2+\sigma_b^2)}}\right] \tag{9}$$

where μ_b,σ_b^2 are the mean and variance value of background and μ_n,σ_n^2 are mean and variance of discussed nth ROI of the image.

4. Experimental Results and Discussion

The suggested method's denoising capabilities are compared with those of the following noise filters in this part using the quantitative and qualitative results: The M1-Hybrid Median Filter (HMF) [15], the M2-Nonlinear Complex Diffusion Filter (NCDF) [25], the M3-Dual Tree Complex Wavelet (DTCWT) using soft thresholding [16], the M4-AWBF, the M5-Anisotropic Coherent Enhancing Diffusion (ACED) [20], the M6-Second-Order Total Generalized Variation Decomposition Filter The values for PSNR, MSE, SSIM, and CNR are used to compare the findings.

Table 1. Quantitative Comparison of Different Filters for Image1.

	PSNR	MSE	SSIM	CNR
M1-HMF	31.7532	43.4272	0.77976	19.1098
M2-NCDF	32.4918	36.6346	0.84563	15.1516
M3-DCTWT	27.2325	122.9784	0.75430	24.9844
M4-AWBF	31.7582	43.3771	0.73565	19.6171
M5-ACED	32.8410	33.8052	0.78402	21.1413
M6-TGVD	26.7554	137.2593	0.74882	14.3477
M7-Proposed	33.6096	29.6549	0.95922	25.6324

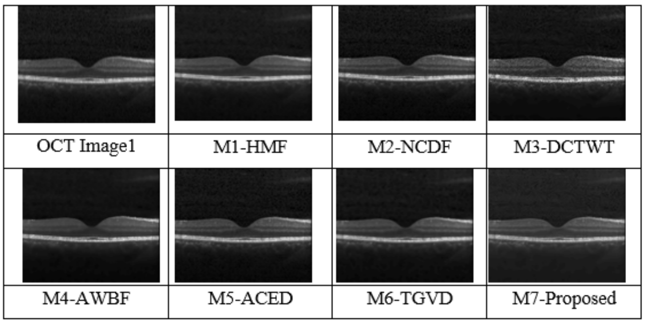

Fig. 1. Ouput denoised images of different filters for OCT Image1.

Table 2. Quantitative Comparison of Different filters for Image2.

	PSNR	MSE	SSIM	CNR
M1-HMF	30.8678	53.2476	0.7619	20.5946
M2-NCDF	30.8988	52.8679	0.8346	27.2027
M3-DCTWT	27.1608	125.0273	0.7487	27.6054
M4-AWBF	29.8727	66.9593	0.6983	19.7385
M5-ACED	32.2760	38.5016	0.7703	23.7114
M6-TGVD	26.7684	136.8480	0.7490	19.3746
M7-Proposed	33.2943	28.3393	0.9557	28.7925

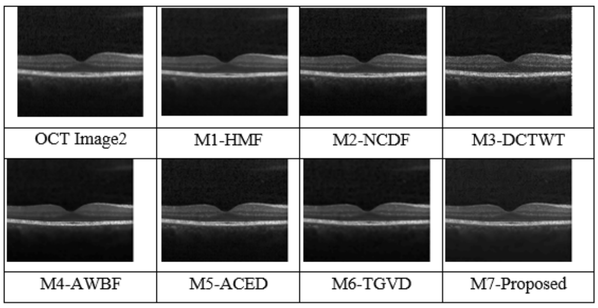

Fig. 2. Output denoised images for OCT Image2.

Table 3. PSNR, MSE, SSIM & CNR values for Image3.

	PSNR	MSE	SSIM	CNR
M1-HMF	31.1096	50.3644	0.7886	20.4535
M2-NCDF	31.7030	43.9319	0.8597	26.9078
M3-DCTWT	25.8223	170.1556	0.7007	25.6809
M4-AWBF	31.2878	48.3389	0.7748	16.3099
M5-ACED	33.2743	30.5951	0.8013	23.6480

M6-TGVD	25.8695	168.3185	0.7610	15.2158
M7-Proposed	33.9355	23.0772	0.9680	28.0387

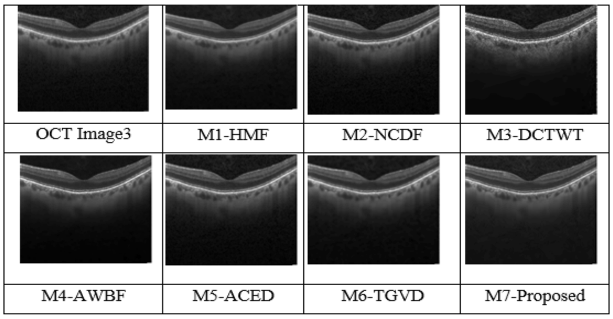

Fig. 3. Output denoised images of different filters for OCT Image3.

Table 4. PSNR,MSE, SSIM & CNR values for Image4.

	PSNR	MSE	SSIM	CNR
M1-HMF	31.2511	48.7494	0.7840	22.9940
M2-NCDF	31.5898	45.0912	0.8515	26.4439
M3-DCTWT	26.3437	150.9082	0.7388	20.6109
M4-AWBF	30.6957	55.3997	0.7549	19.8099
M5-ACED	32.7326	34.6595	0.7931	30.6515
M6-TGVD	24.4638	232.6476	0.7523	18.1366
M7-Proposed	33.8075	24.0665	0.9727	32.0782

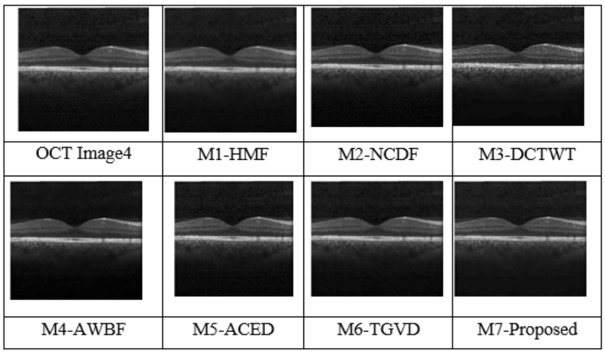

Fig. 4. Output denoised images of different filters for OCT Image4.

Table 5. PSNR, MSE, SSIM & CNR values for Image5.

	PSNR	MSE	SSIM	CNR
M1-HMF	31.7669	43.2898	0.7966	24.0730
M2-NCDF	31.5539	45.4664	0.8589	26.7359
M3-DCTWT	26.5952	142.4150	0.7472	22.0755
M4-AWBF	31.7869	43.0913	0.7763	21.2162
M5-ACED	31.4361	33.1565	0.8026	33.7259
M6-TGVD	25.6024	178.9929	0.7638	16.2525
M7-Proposed	33.0235	32.4132	0.9765	32.1328

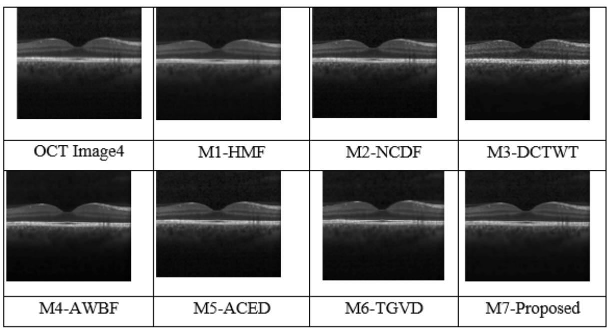

Fig. 5. Output denoised images of different filters for OCT Image5.

Table 6. PSNR, MSE, SSIM & CNR values for Image6.

	PSNR	MSE	SSIM	CNR
M1-HMF	31.2072	49.2446	0.7813	34.4460
M2-NCDF	30.7117	55.1955	0.8417	28.1104
M3-DCTWT	26.7548	137.2786	0.7441	47.8303
M4-AWBF	30.9215	52.5928	0.7619	21.8838
M5-ACED	32.3804	37.5869	0.7823	32.8393
M6-TGVD	26.1052	159.4278	0.7637	16.8254
M7-Proposed	38.6444	8.8845	0.9480	16.1261

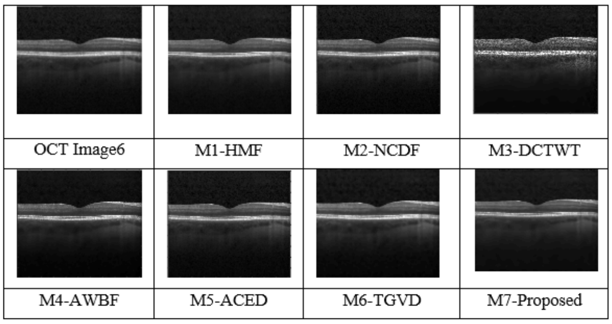

Fig. 6. Output denoised images of different filters for OCT Image6.

Table 7. PSNR, MSE,SSIM & CNR values for Image7.

	PSNR	MSE	SSIM	CNR
M1-HMF	36.6474	14.0716	0.9284	22.2185
M2-NCDF	33.4052	29.6865	0.9518	18.3114
M3-DCTWT	28.6480	88.7739	0.8259	40.7371
M4-AWBF	35.6778	17.5916	0.8655	9.8524
M5-ACED	38.3009	9.6159	0.9311	22.3677
M6-TGVD	25.2056	196.1191	0.8850	6.1865
M7-Proposed	42.2124	3.9069	0.9780	12.9027

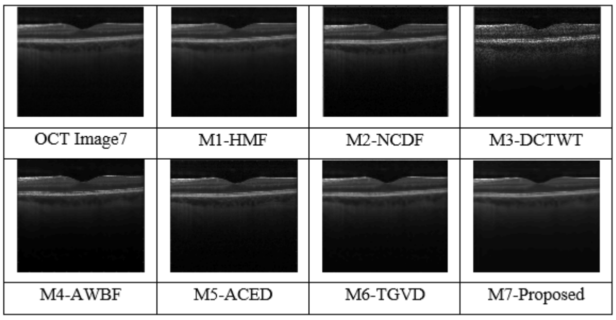

Fig. 7. Output denoised images of different filters for OCT Image7.

Table 8. PSNR, MSE,SSIM & CNR values for Image8.

	PSNR	MSE	SSIM	CNR
M1-HMF	30.3408	60.1169	0.7459	34.9442
M2-NCDF	30.5964	56.6807	0.8227	33.8313
M3-DCTWT	25.3464	189.8648	0.7030	59.1050
M4-AWBF	28.1789	98.8982	0.7294	22.9507
M5-ACED	31.6503	44.4687	0.7586	37.7689
M6-TGVD	25.2597	193.6905	0.7128	19.5767
M7-Proposed	38.6364	8.9009	0.9430	17.0124

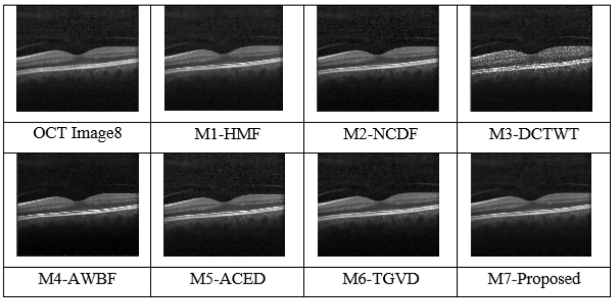

Fig. 8. Output de-noised images of different filters for OCT Image8.

Table 9. PSNR, MSE, SSIM & CNR values for Image9.

	PSNR	MSE	SSIM	CNR
M1-HMF	31.1930	49.4065	0.7826	19.9690
M2-NCDF	29.5964	55.6807	0.8227	32.8313
M3-DCTWT	33.4997	29.0476	0.8599	41.0618
M4-AWBF	31.6639	44.3289	0.7732	17.7401
M5-ACED	32.7438	34.5699	0.7875	23.0163
M6-TGVD	26.6209	141.5773	0.7634	17.2864
M7-Proposed	38.8281	8.5165	0.9503	11.6087

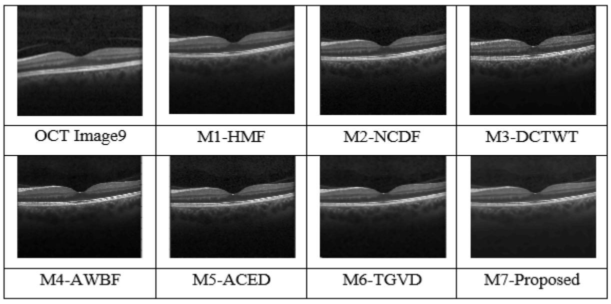

Fig. 9. Output denoised images of different filters for OCT Image9.

Table 10. PSNR, MSE,SSIM & CNR values for Image10.

	PSNR	MSE	SSIM	CNR
M1-HMF	30.2144	61.8923	0.7450	35.0652
M2-NCDF	30.5347	57.4916	0.8199	29.6888
M3-DCTWT	32.9557	32.9236	0.8418	51.4546
M4-AWBF	31.1409	50.0027	0.7453	23.2807
M5-ACED	31.7620	43.3387	0.7534	36.7475
M6-TGVD	25.2031	196.2338	0.7297	18.5763
M7-Proposed	38.2377	9.7567	0.9430	17.5355

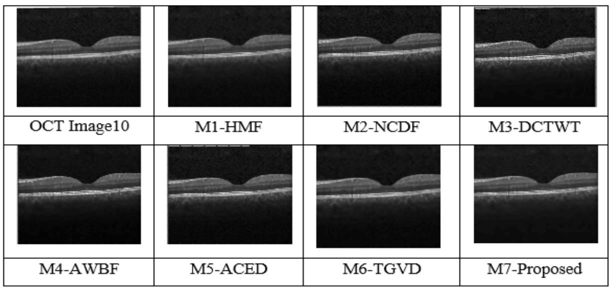

Fig. 10. Output de-noised images of different filters for OCT Image10.

Table 1, Table 2, Table 3, Table 4, Table 5, Table 6, Table 7, Table 8, Table 9 and Table 10 are shown the quantitative comparison of the proposed framework with the six state-of-art filter use for de-speckling the OCT Images for the OCT Image1, Image2, Image3, Image4, and Image5, respectively. From the quantitative result assessment, it is found out that the proposed framework outperform in comparison to all state-of-art filters. The proposed filter has the highest PSNR, SSIM, CNR values, although the value of MSE is the lowest for the proposed framework. These numerical results justify that the proposed framework has a better de-speckling ability and edge, preserving. Similarly, Fig. 1, Fig. 2, Fig. 3, Fig. 4, Fig. 5, Fig. 6, Fig. 7, Fig. 8, Fig. 9 and Fig. 10 show the visual result comparing the proposed framework with the six state-of-art filters. The visual effects also support the quantitative result.

4.1. Comparative Results

Table 1, Table 2, Table 3, Table 4, Table 5, Table 6, Table 7, Table 8, Table 9 and Table 10 are shown the quantitative comparison of the proposed framework with the six state-of-art filter use for de-speckling the OCT images for the OCT Image1, Image2, Image3, Image4, and Image5, respectively. For example for image 1 PSNR value are 31.7532, 32.4918, 27.2325, 31.7582, 32.8410, 26.7554, 33.6096 for filter M1,M2,M3, M4,M5,M6 and M7 respectively that indicate that proposed filter give better enhance image in comparison to compared filter. Same results are obtain for other images also. Similarly comparative Table concluded that proposed method de-noise the images effectively.

5. Conclusion

For the purpose of minimizing the speckle noise encountered in OCT pictures, this proposed framework presented a de-speckling technique. Two distinct types of speckle noise components are filtered differently in this system. For the additive portion of the noise, Wiener filtering is utilised, and for the multiplicative portion, the NSST domain is used. The suggested framework focuses on a different aspect of the image's speckle noise independently. The multiscale and multidirectional analysis of filtered pictures is carried out by the NSST domain. The high amplitude noise components were suppressed by the diffusion process in the suggested framework, and edge preservation is improved by thresholding. The suggested system's capacity for denoising is enhanced by this collaborative process. On OCT images and conventional test images, the proposed framework has also contrasted the quantitative and qualitative findings with those from other cutting-edge filters. According to the experimental findings, the suggested approach reduces speckle noise more effectively than any other filters while also having greater edge preservation abilities.

References

1. Bowd C, Weinreb RN, Williams JM, Zangwill LM. The retinal nerve fiber layer thickness in ocular hypertensive, normal, and glaucomatous eyes with optical coherence tomography. *Archives of Ophthalmology,* 118(1), 2000, pp. 22-6.
2. Medeiros FA, Zangwill LM, Bowd C, Vessani RM, Susanna Jr R, Weinreb RN. Evaluation of retinal nerve fiber layer, optic nerve head, and macular thickness measurements for glaucoma detection using optical coherence tomography. *American Journal of Ophthalmology*, 139(1), 2005, pp. 44-55.
3. Srinivasan VJ, Wojtkowski M, Witkin AJ, Duker JS, Ko TH, Carvalho M, Schuman JS, Kowalczyk A, Fujimoto JG. High-definition and 3-dimensional imaging of macular pathologies with high-speed ultrahigh-resolution optical coherence tomography. *Ophthalmology*, 113(11), 2006, pp. 2054-65.
4. Farsiu S, Chiu SJ, O'Connell RV, Folgar FA, Yuan E, Izatt JA, Toth CA, Age-Related Eye Disease Study 2 Ancillary Spectral Domain Optical Coherence Tomography Study Group. Quantitative classification of eyes with and without intermediate age-related macular degeneration using optical coherence tomography. *Ophthalmology*, 121(1), 2014, pp. 162-72.
5. Chiu SJ, Izatt JA, O'Connell RV, Winter KP, Toth CA, Farsiu S. Validated automatic segmentation of AMD pathology including drusen and geographic atrophy in SD-OCT images. *Investigative Ophthalmology & Visual Science*, 53(1), 2012, pp. 53-61.
6. Schuman SG, Koreishi AF, Farsiu S, Jung SH, Izatt JA, Toth CA. Photoreceptor layer thinning over drusen in eyes with age-related macular degeneration imaged in vivo with spectral-domain optical coherence tomography. *Ophthalmology*, 116(3), 2009, pp. 488-96.
7. Ozcan A, Bilenca A, Desjardins AE, Bouma BE, Tearney GJ. Speckle reduction in optical coherence tomography images using digital filtering. *JOSA* A, 24(7), 2007, pp. 1901-10.
8. Adler DC, Ko TH, Fujimoto JG. Speckle reduction in optical coherence tomography images by use of a spatially adaptive wavelet filter. *Optics Letters*, 29(24), 2004, pp. 2878-80.
9. Sudeep PV, Niwas SI, Palanisamy P, Rajan J, Xiaojun Y, Wang X, Luo Y, Liu L. Enhancement and bias removal of optical coherence tomography images: An iterative approach with adaptive bilateral filtering. *Computers in Biology and Medicine*, 71, 2016, pp. 97-107.
10. Mirzapour F, Ghassemian H. Multiscale Gaussian derivative functions for hyperspectral image feature extraction. *IEEE Geoscience and Remote Sensing Letters*, 13(4), 2016, pp. 525-9.
11. Du Y, Liu G, Feng G, Chen Z. Speckle reduction in optical coherence tomography images based on wave atoms. *Journal of Biomedical Optics*, 19(5), 2014, pp. 056009-.
12. Kafieh R, Rabbani H, Selesnick I. Three dimensional data-driven multi scale atomic representation of optical coherence tomography. *IEEE Transactions on Medical Imaging*, 34(5), 2014, pp. 1042-62.
13. Duan J, Lu W, Tench C, Gottlob I, Proudlock F, Samani NN, Bai L. Denoising optical coherence tomography using second order total generalized variation decomposition. *Biomedical Signal Processing and Control*, 24, 2016, pp. 120-7.
14. Ren H, Qin L, Zhu X. Speckle reduction and cartoon-texture decomposition of ophthalmic optical coherence tomography images by variational image decomposition, *Optik*, 127(19), 2016, pp. 7809-21.
15. Baghaie A, D'souza RM, Yu Z. Application of independent component analysis techniques in speckle noise reduction of retinal OCT images. *Optik*, 127(15), 2016, pp. 5783-91.
16. Amini Z, Rabbani H. Optical coherence tomography image denoising using Gaussianization transform. *Journal of Biomedical Optics*, 22(8), 2017, pp. 1-12.
17. Fang L, Li S, Cunefare D, Farsiu S. Segmentation based sparse reconstruction of optical coherence tomography images. *IEEE transactions on medical imaging*, 36(2), 2016, pp. 407-21.
18. Anantrasirichai N, Nicholson L, Morgan JE, Erchova I, Mortlock K, North RV, Albon J, Achim A. Adaptive-weighted bilateral filtering and other pre-processing techniques for optical coherence tomography. *Computerized Medical Imaging and Graphics*, 38(6), 2014, pp. 526-39.
19. Guariglia E, Silvestrov S. Fractional-Wavelet Analysis of Positive definite Distributions and Wavelets on D'(C) D′(C). InEngineering Mathematics II: Algebraic, Stochastic and Analysis Structures for Networks, Data Classification and Optimization. *Springer International Publishing*, 2016, pp. 337-353
20. Guariglia E. Spectral analysis of the Weierstrass-Mandelbrot function. *In 2017 2nd International Multidisciplinary Conference on Computer and Energy Science (SpliTech), IEEE*, 2017, pp. 1-6.
21. Raj SA, Nair MS, Subrahmanyam GR. Satellite image resolution enhancement using nonsubsampled contourlet transform and clustering on subbands. *Journal of the Indian Society of Remote Sensing,* 45, 2017, pp. 979-91.
22. Wu YQ, Yin J, Dai YM. Image enhancement in NSCT domain based on fuzzy sets and artificial bee colony optimization. *Journal of South China University of Technology (Natural Science Edition)*, 43(1), 2015, pp. 59-65.
23. Da Cunha AL, Zhou J, Do MN. The nonsubsampled contourlet transform: theory, design, and applications. *IEEE transactions on image processing*, 15(10), 2006, pp. 3089-101.
24. Aili W, Ye Z, Shaoliang M, Mingji Y. Image denoising method based on curvelet transform. *In 2008 3rd IEEE Conference on Industrial Electronics and Applications*, 2008, pp. 571-574.
25. Bao P, Zhang L. Noise reduction for magnetic resonance images via adaptive multiscale products thresholding. *IEEE Transactions on Medical Imaging*, 22(9), 2003, pp. 1089-99.